# Characterization of i-PP Shear-Induced Crystallization Layers Developed in a Slit Die

**Marcelo Farah, Rosario E. S. Bretas**

*Department of Materials Engineering, Universidade Federal de São Carlos, 13565-905 São Carlos, SP, Brazil*

Received 24 March 2003; accepted 24 June 2003

**ABSTRACT:** In this work, the shear-induced crystalline layers of isotactic polypropylene (i-PP), developed in a slit die, were characterized by different techniques. Rheological studies made in a strain-controlled rheometer, at different crystallization temperatures, $T_c$, allowed us to observe that the induction time for the beginning of the shear-induced crystallization, $t_i$, decreased as the shear rate increased, whereas at a given shear rate, the higher the $T_c$, the higher the $t_i$. The thickness of the shear-induced crystallized layer, after extrusion through the slit die, was found to decrease with the increase of the die temperature, $T_d$, at a given flow rate, $Q$, and to increase with the increase in $Q$, at a given $T_d$. Regarding the die length, it was found that only at $T_d$ = 169°C, the thickness of this layer increased with the length. By polarized light optical microscopy (PLOM), five different crystalline layers were observed along the thickness of the sample. By scanning and transmission electron microscopy (SEM and TEM), respectively, and wide-angle X-rays (WAXS), it was found that layer 1, the nearest to the wall, was formed mainly by very small and oriented $\alpha$-crystallites, while layer 2 was mainly composed of $\beta$-crystallites; also it was found that the amount of the $\beta$-phase decreased as the shear rate decreased. © 2004 Wiley Periodicals, Inc. J Appl Polym Sci 91: 3528–3541, 2004

**Key words:** crystallization; polypropylene; morphology; rheology; extrusion

## INTRODUCTION

The morphology along the thickness of semicrystalline polymers after extrusion or injection molding is usually formed by crystalline layers of different sizes and forms. Near the wall, very small and highly extended crystallites or cylindrites are observed, while near the center, large and unoriented spherulites are seen. In the intermediate region, columnar- or transcrystalline-type crystals can be observed. This morphology is called skin-core type. The skin is highly oriented due to the large shear rates that are developed near the wall, while the core is spherulitic because of the zero or minimum shear rates. This skin is also known as the shear-induced crystalline layer, while the core is known as the quiescent crystalline layer. The effect of the shear rate gradient on the morphology can also be better visualized in the injection molding of immiscible polymer blends,[1] where the disperse phase deforms according to this gradient. Although it is known that elongational flows enhance crystallization better than shear flows,[2,3] we will limit in this work to the study of only shear-induced crystallization.

Eder et al.[4] were one of the first to formulate a kinetic theory for the development and understanding of this shear-induced crystalline layer. Their main assumptions were that the surfaces or precursors at which nucleation could start were created by the flow and they did not exist prior to the onset of the flow. These precursors also would disappear by relaxation, after the stop of the flow. However, if the sheared melt were quickly cooled, shear-induced crystallization would occur. Their model allowed them to estimate the size of the flow-induced layers. Recently, Doufas et al.[5] presented a continuum model for this flow-induced crystallization, which combined thermodynamics with the Avrami equation. Their model had two constitutive equations: one for the amorphous phase and the other for the crystalline one, which was coupled with the crystallization kinetics. The melt was modeled as a Giesekus material and the crystalline phase was modeled as a collection of multibead rigid rods that grew and were oriented in the flow field. Their basic assumption was that the melt was homogeneous; that is, all polymer chains were considered to crystallize in the same manner and, therefore, to have the same degree of crystallinity at any time. The model did not account, however, for any morphological details (spherulitic, folded/lamellar, or fibrillar microstructures).

One of the polymers that more easily forms this type of multilayer morphology after extrusion or injection molding is isotactic polypropylene (i-PP). Thus, it constitutes a very useful polymer to make studies of shear-induced crystallization.

*Correspondence to:* R. E. S. Bretas (bretas@power.ufscar.br).

Journal of Applied Polymer Science, Vol. 91, 3528–3541 (2004)

Studies of the quiescent isothermal and nonisothermal crystallization of i-PP has been intense.[6,7,8] As it is known, i-PP can form three types of crystalline structures after quiescent crystallization: the $\alpha$-phase, with a monoclinic unit cell; the $\beta$-phase, with a pseudohexagonal unit cell[9]; and the $\gamma$-phase, with an orthorhombic unit cell.[10] The $\alpha$-phase, the most common, can form three different types of spherulites[11,6]: type I, below a crystallization temperature, $T_c$, of 134°C; type II, above $T_c$ = 137°C; and a mixed type, in the intermediate region between 134 and 137°C. Two types of $\beta$-spherulites can also be formed[11,6]: type II, below $T_c$ = 128°C (highly birefringent); and type IV, between 128 and 132°C. Varga,[6] in his comprehensive review, also pointed out that the formation of $\beta$-PP crystals had a theoretical upper temperature limit, called $T_{\beta\alpha}$ = 140–141°C, and a lower temperature limit, called $T_{\alpha\beta}$ = 100°C; also he pointed out that when $T_c < T_{\beta\alpha}$, the crystallization growth rate of the $\beta$-phase, $G_\beta$, was higher than the crystallization growth rate of the $\alpha$-phase, $G_\alpha$. For the case of shear-induced crystallization, Varga demonstrated[6] that, in the case of i-PP, during application of a shear stress, parts of the i-PP macromolecules would orient, forming row nuclei. These row nuclei would begin to grow at a higher temperature than the homogeneous or heterogeneous ones,[6]thus forming cylindrites of $\alpha$-phase, because the crystallization had started at a high temperature, above $T_{\beta\alpha}$. At high degree of under cooling, that is, $(T_m - T_c)$, where $T_m$ is the melting temperature; however, punctiform $\beta$-nuclei might also be formed on an $\alpha$-row nucleus or on the growing $\alpha$-cylindritic front.

Varga and Karger-Kocsis[12] modeled the skin region, calling it the row-nucleated cylindritic region. They established that the shearing of the melt first yielded $\alpha$-row nuclei. The surface of these $\alpha$-nuclei was covered by a point such as $\beta$-nuclei; therefore, this surface could induce an $\alpha$- to $\beta$-transition, that is, an $\alpha\beta$-secondary nucleation. These $\beta$-nuclei would induce the growth of $\beta$-spherulitic segments. This $\beta$-spherulitic growth would terminate the growth of the primary $\alpha$-cylindritic front because this front had reached a $T_c < T_{\beta\alpha}$, where $G_\beta > G_\alpha$.

Recent work[13] using wide-angle X-rays (WAXS) and small-angle X-rays (SAXS), upon application of a step shear rate, showed that the i-PP molecules aligned in the flow direction, which enhanced primary nucleation and caused growth of lamellae perpendicular to the flow direction. As crystallization proceeded, discrete X-ray reflections appeared indicating the presence of $\alpha$- and $\beta$-phases; it seemed that the $\beta$-phase crystallites were unoriented and located in between the oriented cylindrites of the $\alpha$-phase. Other WAXS studies[14] have shown that the $\beta$-phase can also gradually be transformed into a highly oriented, conformational disordered $\alpha$-phase as the strain increases.

Another work,[15] in which a rheometer was used to monitor shear-induced crystallization, found that the sheared and no sheared samples had WAXS reflections of the $\alpha$- and $\beta$-phases. Few highly birefringent $\beta$-spherulites were found among a majority of $\alpha$-spherulites. Other recent studies[16] have been capable of monitoring the development of the crystallinity fraction under shear of i-PP by using a rheometer coupled with a differential thermal analyzer (DTA).

Experiments of injection molding performed in our labs[17] have shown that the $\beta$-phase of i-PP appears only when high-injection flow rates are used, independent of the mold temperature.

In the present work, the shear-induced crystalline layers of i-PP after extrusion in a slit die were characterized by different techniques.

## EXPERIMENTAL

### Materials

An iPP of $M_w$ = 448,800 g/mol, melt flow index (MFI) = 4.5 g/10 min, from OPP Petroquímica (Triunfo, RS, Brazil) was used in this work.

### Rheological characterization

The shear viscosity of the iPP, $\eta(\dot{\gamma})$, at high shear rates, was measured in a capillary rheometer, from Instron, model 4467; the diameter of the capillary was 0.04 in. and the length was 2 in. The measurements were done at 190, 200, 215, and 230°C. A power law model, $\eta(\dot{\gamma}) = m\dot{\gamma}^{n-1}$, where $m$ is the consistency and $n$ is the power law index, was assumed for the shear viscosity.

The induction times for the beginning of the shear-induced crystallization, $t_i$, were measured in a strain-controlled rheometer, ARES, from Rheometrics, by using a parallel plates geometry. The diameter of the plates was 25 mm and the gap was 0.9 mm. The samples for this characterization were prepared by compression molding, at 220°C, for 5 min, under a pressure of 5 ton. The samples were put between the rheometer plates, heated for 12 min, at 220°C, under $N_2$ atmosphere, and cooled down to the crystallization temperature, $T_c$, of 140, 145, or 150°C at a cooling rate of approximately 10°C/min. After $T_c$ was reached, and the melt was sheared at 5, 7, 10, or 15 $s^{-1}$, while monitoring the shear stress, $\tau$. The test was interrupted when the security torque of the transducer was attained.

### Extrusion

To obtain shear-induced crystallization samples at high shear rates, experiments with a slit die, similar to the Eder et al.[4] and Isayev et al.[18] experiments, were done. The slit die, made of aluminum, was coupled to

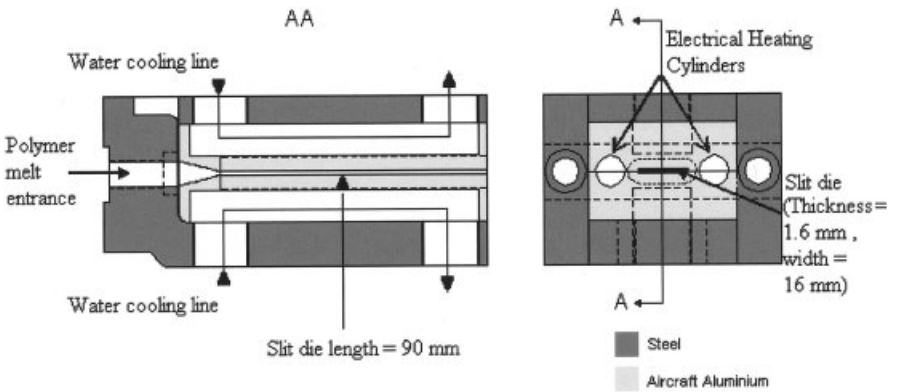


**Figure 1** Slit die used in this work.

a twin-screw extruder ZK30 (Werner and Pfleider); its dimensions are shown in Figure 1.

The thickness of the slit die, $2H$, was 1.6 mm, the width $W$ was 16 mm, and the length $L$ was 90 mm. Due to contraction, the samples had a final thickness of between 1.45 and 1.6 mm, after cooling.

The feeding mass rate of the extruder, $Q$, also called flow rate, was automatically set to 2, 3.15, 4.3, 5.45, 6.6, 7.75, 8.9, and 10.05 Kg/h; the screw rotation was set at 175 rpm. The extruder temperature profile was 200, 220, 230, 230, 230, 230, and 230°C. The die temperatures, $T_d$, were set at 169, 178, 190, 200, 215, and 230°C.

After obtaining a constant $Q$, the flow was ceased for 12 min, to erase the previous thermomechanical history of the melt. Then, it was again reinitiated, and after a constant pressure die was obtained, the extruder heating system was disconnected, and simultaneously, the cooling system was activated. Circulating water into the cooling channels made the cooling. The cooling time was monitored by using a thermocouple from Omega, with a thickness of 0.0762 mm, put between the central parts of the die and coupled to a microcomputer from National Instruments, NI-DAQ, with the accessories SC-2345 and SCC-TC02. The opening of the die to remove the shear-induced crystalline samples was done after 3 min of cooling.

Each sample was cut into eight different sections, areas named after the work of Isayev et al.,[18] as shown in Figure 2.

Each area had a length of 1 cm; they were microtomed with a diamond knife to produce films of thickness of 20 $\mu$m each, perpendicular to the flow direction, by using a microtome Microm, model HM360. These areas were numbered from 1 to 8, 1 being the area nearest the die entrance.

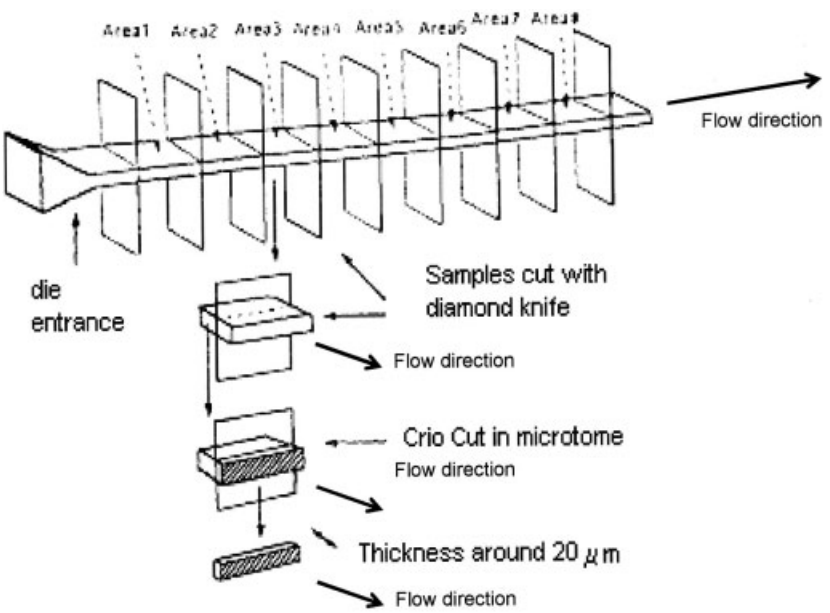


**Figure 2** Preparation of the shear-induced crystalline samples after extrusion.

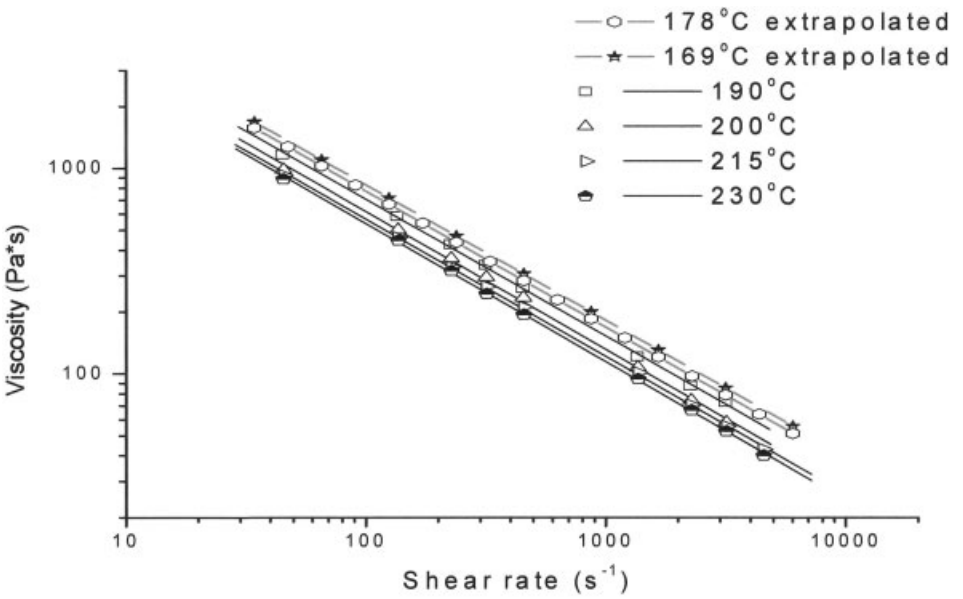


**Figure 3** Shear viscosity curves of the iPP at different temperatures.

### Polarized light optical microscopy (PLOM)

The morphology of the microtomed films was observed in a polarized light optical microscope Leica, model DMRXP.

### Scanning and transmission electron microscopy

The morphology of the microtomed films was also observed by scanning electron microscopy (SEM) and transmission electron microscopy (TEM). The SEM equipment was a H-S45000 FEG, from Hitachi, and the TEM equipment was CM200, from Phillips.

The samples for TEM and SEM were prepared by chemical etching. These samples were microtomed films of each area, parallel to the flow direction. The chemical etching was done with sulfuric acid and potassium permanganate. After the etching, a replica was obtained, after Pt and C deposition.

### Wide-angle x-rays

The measurements of WAXS were done between $5 < 2\theta < 50°$, at a scanning of 0.02°/s in X-ray equipment from Phillips PW 1140/90, under Cu radiation. X-ray diffraction measurements were made first in the surfaces of the samples. After these measurements, the sample surfaces were polished with 600-mesh sandpaper to remove layers of 58, 118, 181, and 255 $\mu$m. The resultant thickness was measured with a micrometer Mitutoyo, with an accuracy of 1 $\mu$m. After each layer was removed, X-ray diffraction was done on the resultant surface.

## RESULTS AND DISCUSSION

### Rheological characterization

At 169 and 178°C, the $\eta(\dot{\gamma})$ of the i-PP was not measured because the stress values were higher than the transducer limit of the capillary rheometer. Therefore, the parameters of the power law model, $n$ and $m$, at these two temperatures, were obtained by extrapolation. For this extrapolation, the temperature dependence of $\eta(\dot{\gamma})$ was assumed to be Arrhenius type, or $\eta(T) = Ae^{E/RT}$, where $A$ is a constant and $E$ is the flow activation energy. From the experimental measurements at the other temperatures, $E$ was found to be equal to 197.62 J/mol. Thus, the values of $\eta(\dot{\gamma})$ at 100, 500, and 1000 $s^{-1}$, at 169 and 178°C, were calculated and plots of $\eta(\dot{\gamma})$ at 169 and 178 were thus obtained. Figure 3 shows these results and Table I shows the power law parameters, $n$ and $m$.

It is observed that $n$ was independent of temperature and approximately equals 0.33.

Figure 4(a, b, c) shows the behavior of the shear stress as a function of time after a predefined $\dot{\gamma}$ was

**TABLE I**
**Power Law Parameters, $n$ and $m$ for i-PP, at Different Temperatures**

| Temperature (°C) | $n$ | $m$ (Pa $s^n$) |
|---|---|---|
| 169 | 0.3403 | 17,400.83 |
| 178 | 0.3375 | 16,417.61 |
| 190 | 0.3348 | 15,142.24 |
| 200 | 0.3288 | 13,509.07 |
| 215 | 0.3321 | 12,268.74 |
| 230 | 0.3271 | 11,954.19 |

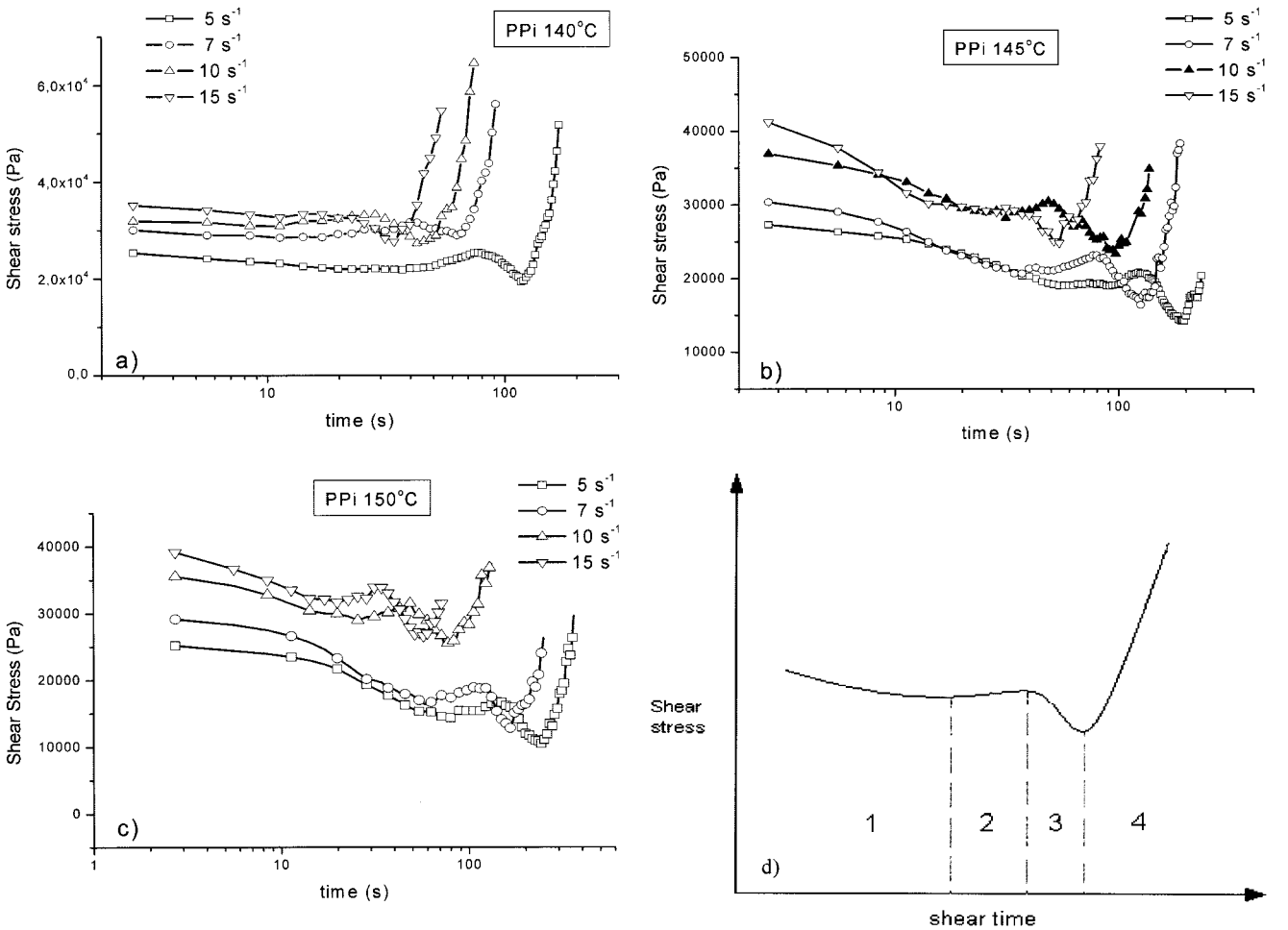


**Figure 4** Induction times for the beginning of the shear-induced crystallization, as obtained by rheometry: (a) $T_c$ = 140°C; (b) $T_c$ = 145°C; (c) $T_c$ = 150°C; (d) scheme of the four regions.

applied, at different $T_c$'s in the strain-controlled rheometer. It can be observed that, independently of the crystallization temperature, the curves displayed four distinct regions in which $\tau$ behaved differently with respect to time, as shown schematically in Figure 4(d). Region 1 was observed at low shear times, where $\tau$ was constant or slightly decreased with time. The slight decrease can be attributed to melt disentanglement. Region 2 was observed at intermediate times, where $\tau$ increased with time because of the beginning of crystallization (nucleation). Region 3 occurred at higher times, where $\tau$ again decreased with time. This last decrease can be attributed to the fact that, being the crystallization an exothermic transformation, an increase of local temperature will occur, therefore, decreasing $\eta(\dot{\gamma})$and $\tau$. Finally, region 4 occurred at still higher times, where $\tau$ increased again with time, rapidly, because of crystal growth (more solid material is present). We assumed that $t_i$ corresponded to the time where region 2 began.

This scheme can be compared with the model of McHugh and collaborators.[5]In their model, they used a parameter called $\xi$ to couple the crystallinity with the conformation tensor $\mathbf{c} \equiv \langle \mathbf{RR} \rangle$, where $\mathbf{R}$ is the end-to-end vector of the amorphous portion of the chains; the degree of coupling on the shear stress, after

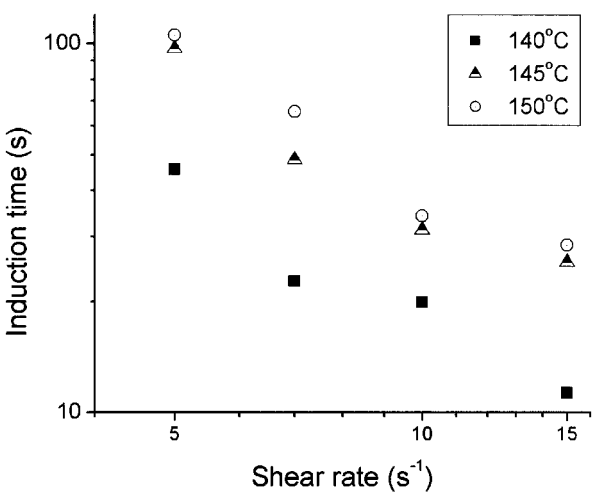


**Figure 5** Induction time for the beginning of the shear-induced crystallization as a function of the shear rate.

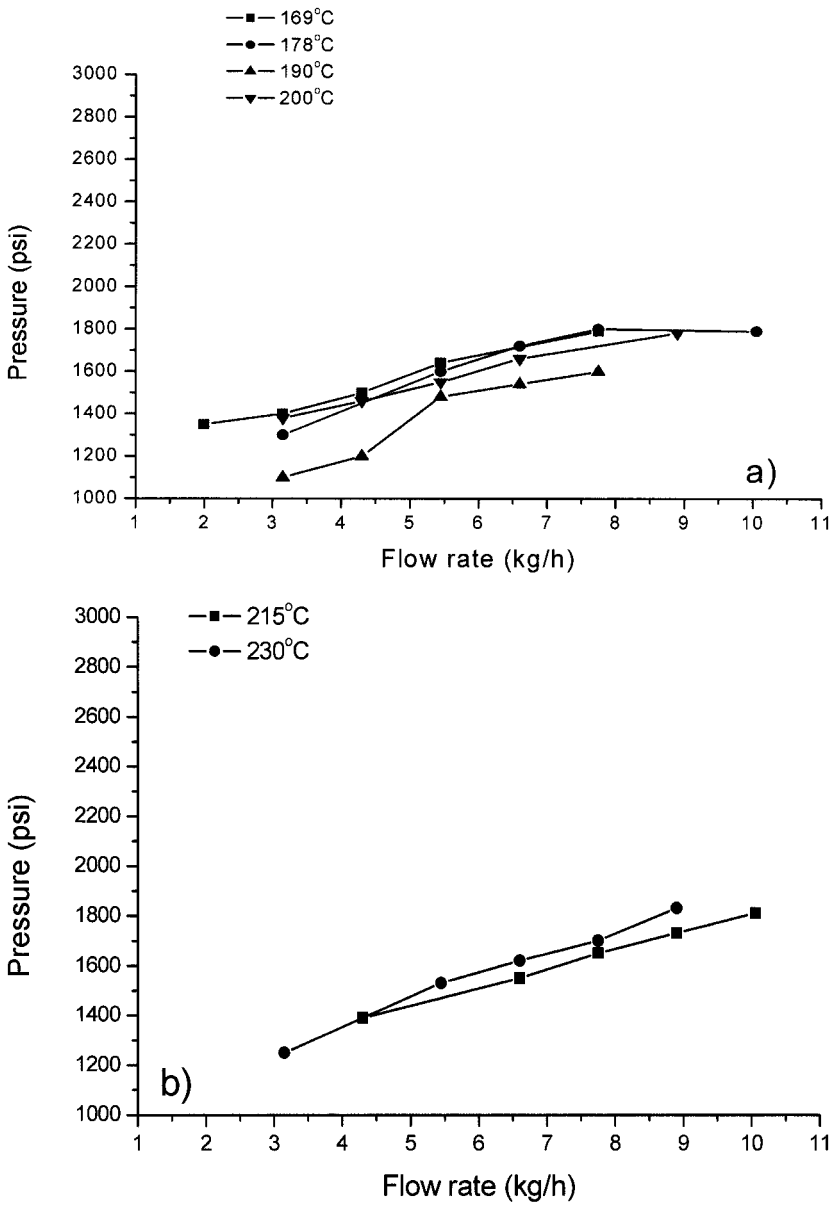


**Figure 6** Flow rate as a function of the die pressure and temperature: (a) Points where flow-induced crystallization was observed; (b) points where no flow crystallization was observed.

applying a shear rate of 30 s, showed that for $\xi = 2$, a stress overshoot was observed after the initial stages of the melt deformation, followed by the flow-induced crystallization, after which the shear stress increased to levels higher than of the melt, in the same way as our results.

The $t_i$ values are shown in Figure 5.

It can be observed from this figure that, at a given $T_c$, the induction time decreased as the shear rate increased; also it is observed that the higher the $T_c$, at a given shear rate, the higher the induction time. Earlier studies[4,5] found that the induction times versus shear rate curves had two stages. In the first stage, the induction times were independent of the shear rate; this stage would represent the onset of spherulitic crystallization. In the second stage, the induction times decreased with the shear rate, representing the shear-induced crystallization. In our rheological studies, only the second stage was observed, thus confirming shear-induced crystallization.

### Extrusion

The $x$-component of the velocity, $v_x(y)$, of a power law fluid in a slit die can be represented as having a plug type profile.

This profile or velocity gradient and the corresponding flow rate $Q$ can be calculated[19] by the equations:

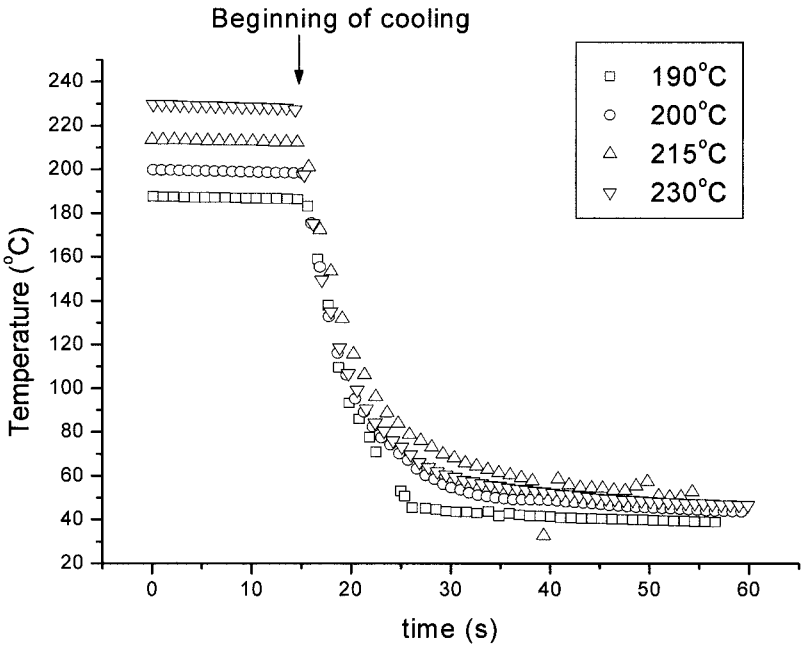


**Figure 7** Cooling times profiles of the slit die.

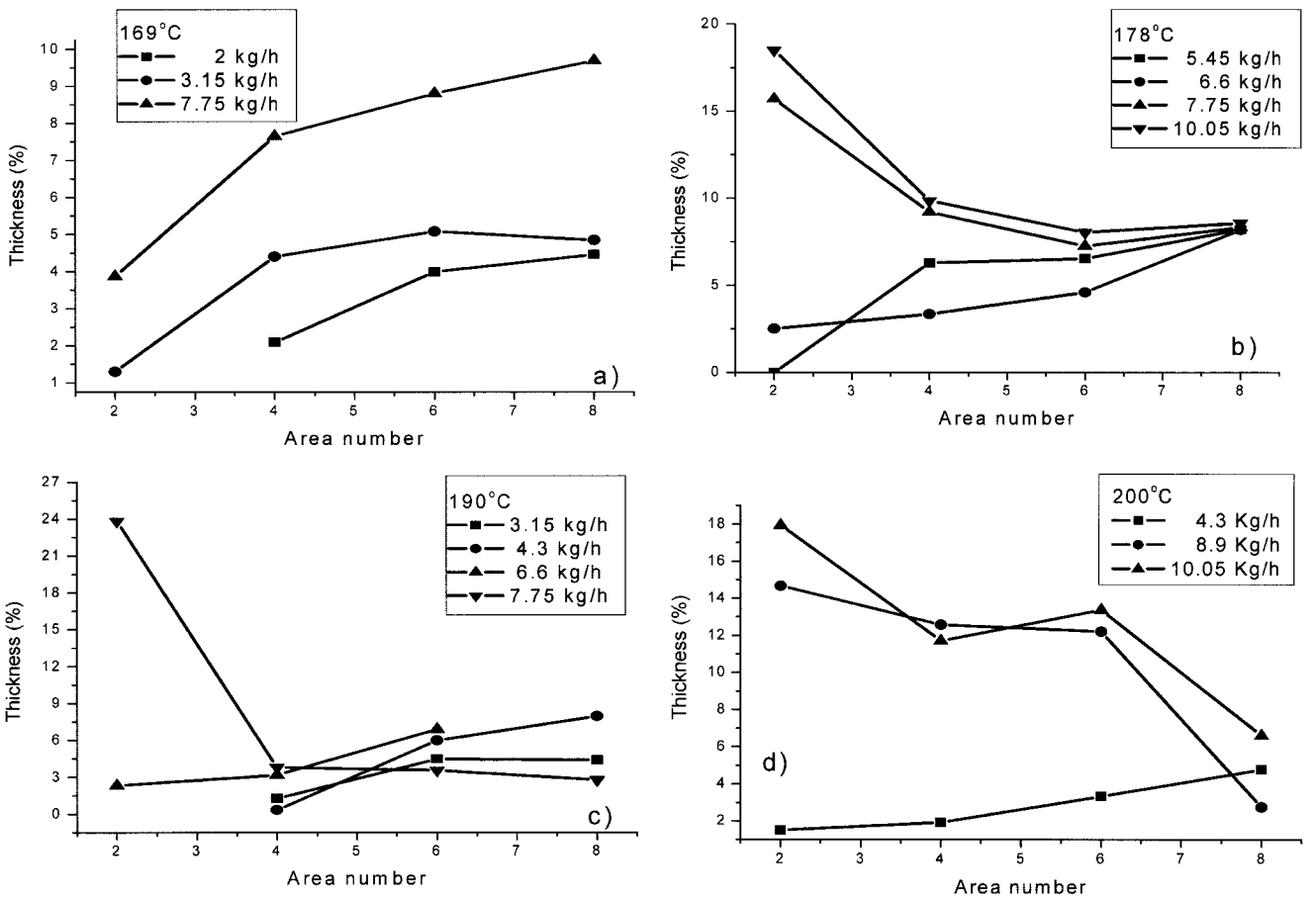


**Figure 8** Thickness of the flow-induced crystallized layer as a function of the die length, at different temperatures: (a) 169°C, (b) 178°C, (c) 190°C, and (d) 200°C.

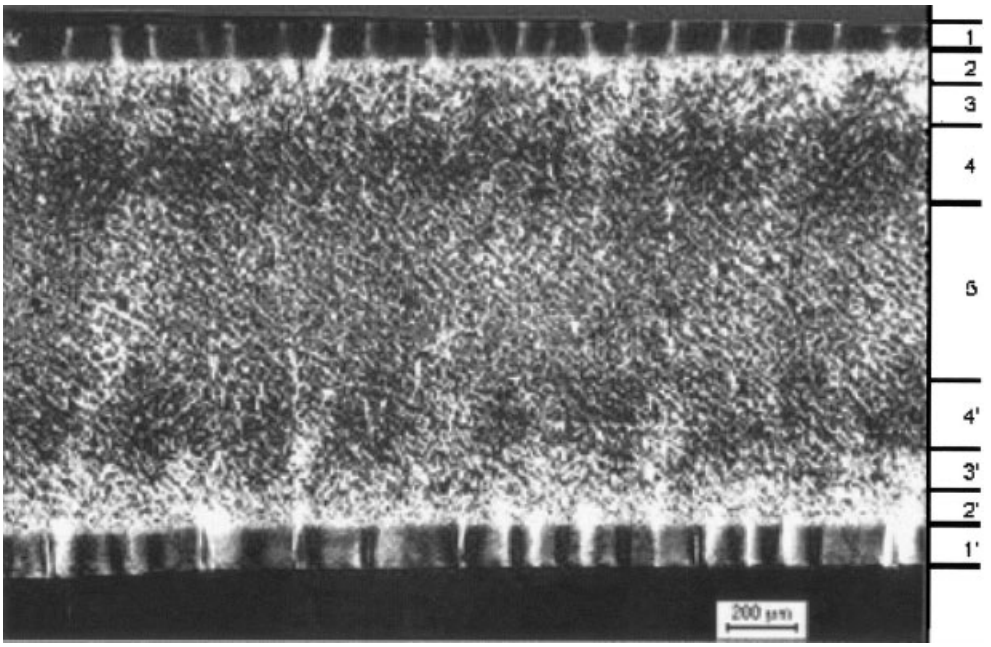


**Figure 9** PLOM micrograph of a whole sample, extruded at $T_d$ = 200°C, $Q$ = 8.9 kg/h, area number 5.

$$v_x = \frac{nH}{n+1}\left(\frac{H\Delta P}{mL}\right)^{1/n}\left[1-\left(\frac{y}{H}\right)^{(n+1)/n}\right] \quad (1)$$

$$Q = \frac{2n}{2n+1}WH^2\left(\frac{H\Delta P}{mL}\right)^{1/n} \quad (2)$$

The shear rate $\dot{\gamma}_{xy}(y)$, on the other hand, can be calculated from the relation:

$$\dot{\gamma}_{xy} = \frac{\partial v_x}{\partial y} \quad (3)$$

It can be observed that as $\Delta P$ increases, $Q$ and also $\dot{\gamma}_{xy}$ increase. It can also be observed that as $n$ decreases, the height of the central part of the velocity profile (the plug) increases as well as the wall velocity gradient.[19,20]

In our case, $n$ = 0.33, as already mentioned; thus, the maximum shear rate will occur very close to the wall. Then, at constant $Q$, the shear-induced crystallization will occur first at this point of maximum shear rate. We also observed from our rheological studies that at a constant shear rate, as $T_c$ increased, $t_i$ also increased. In other words, at constant $Q$, if $T_c$ increases, the thickness of the flow-induced crystalline layer at a given point will be expected to decrease.

On the other hand, at a constant $T_c$, as $Q$ increases (or $\dot{\gamma}_{xy}$ increases), $t_i$ will decrease and the thickness of this layer at a given point will be expected to increase.

**TABLE II**
**Values of the Thickness of Area Number 6 as a Function of $T_d$ at a Given $Q$**

| $Q$ (kg/h) | $T_d$ (°C) | Thickness (%) |
|---|---|---|
| 3.15 | 169 | 4 |
| | 190 | 4.5 |
| 4.3 | 190 | 6 |
| | 200 | 3.2 |
| 6.6 | 178 | 4.0 |
| | 190 | 6.1 |
| 7.75 | 169 | 8.5 |
| | 178 | 7.5 |
| | 190 | 3.0 |
| 10.05 | 178 | 8.0 |
| | 200 | 6.8 |

**TABLE III**
**Values of the Thickness of Area Number 6 as a Function of $Q$, at a Given $T_d$**

| $T_d$ (°C) | $Q$ (kg/h) | Thickness (%) |
|---|---|---|
| 169 | 2 | 4 |
| | 3.15 | 4 |
| | 7.75 | 8.5 |
| 178 | 5.45 | 6.5 |
| | 6.6 | 4.0 |
| | 7.75 | 7.5 |
| | 10.05 | 8.0 |
| 190 | 3.15 | 4.5 |
| | 4.3 | 6.0 |
| | 6.6 | 6.1 |
| | 7.75 | 3.0 |
| 200 | 4.3 | 3.2 |
| | 8.9 | 3.0 |
| | 10.05 | 6.8 |

**TABLE IV**
**Approximated Thickness of the Layers of the Sample of Figure 10**

| Layer | 1 | 2 | 3 | 4 | 5 |
|---|---|---|---|---|---|
| Thickness ($\mu$m) | 84–126 | 73–84 | 126–136 | 210–213 | 547–558 |

Thus, in our work, two situations will be analyzed: (1) constant $Q$ with increasing $T_c$ (or $T_d$) and (2) constant $T_c$ (or $T_d$) with increasing $Q$.

Figure 6(a) shows $Q$ as a function of the die pressure and temperature; the points where no shear-induced crystallization was observed are shown in Figure 6(b). As expected from eq. (2), $Q$ increased as $\Delta P$ increased. It can also be observed that above 200°C, no shear-induced crystallization occurred.

Figure 7 shows the die cooling profiles; it can be observed that the die cooling to room temperature took place between 10 and 25 s. It can also be observed that the higher the $T_d$, the higher the cooling rate.

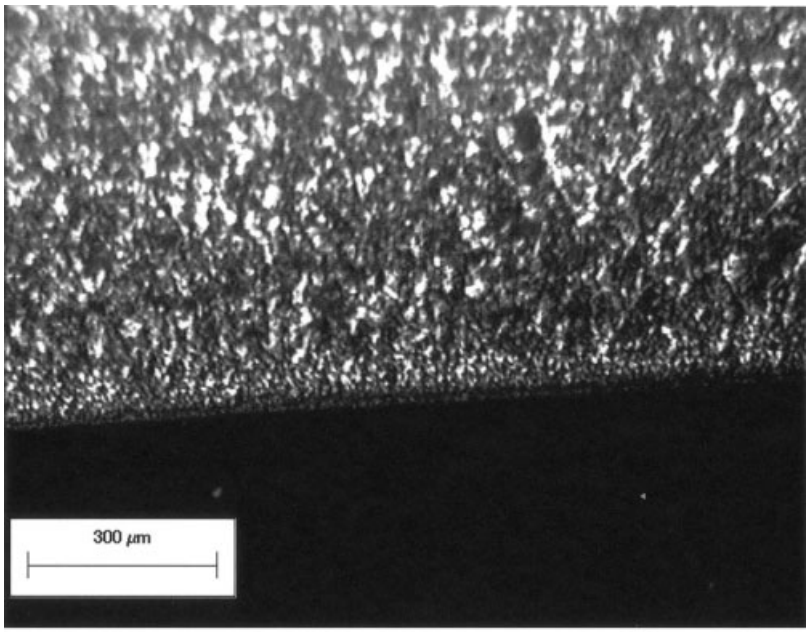


(a)

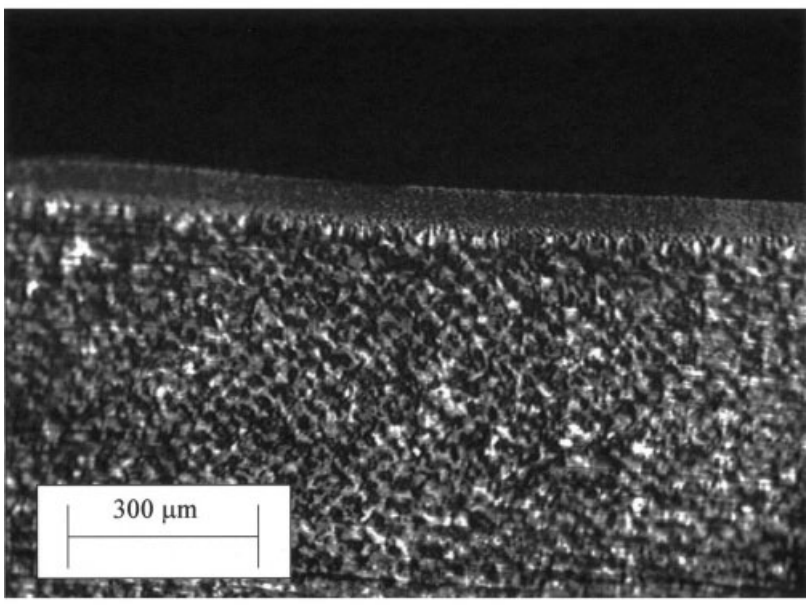


(b)

**Figure 10** Samples extruded at a $T_d$ = 169°C and $Q$ = 2 kg/h. Area numbers: (a) 4, (b) 6.

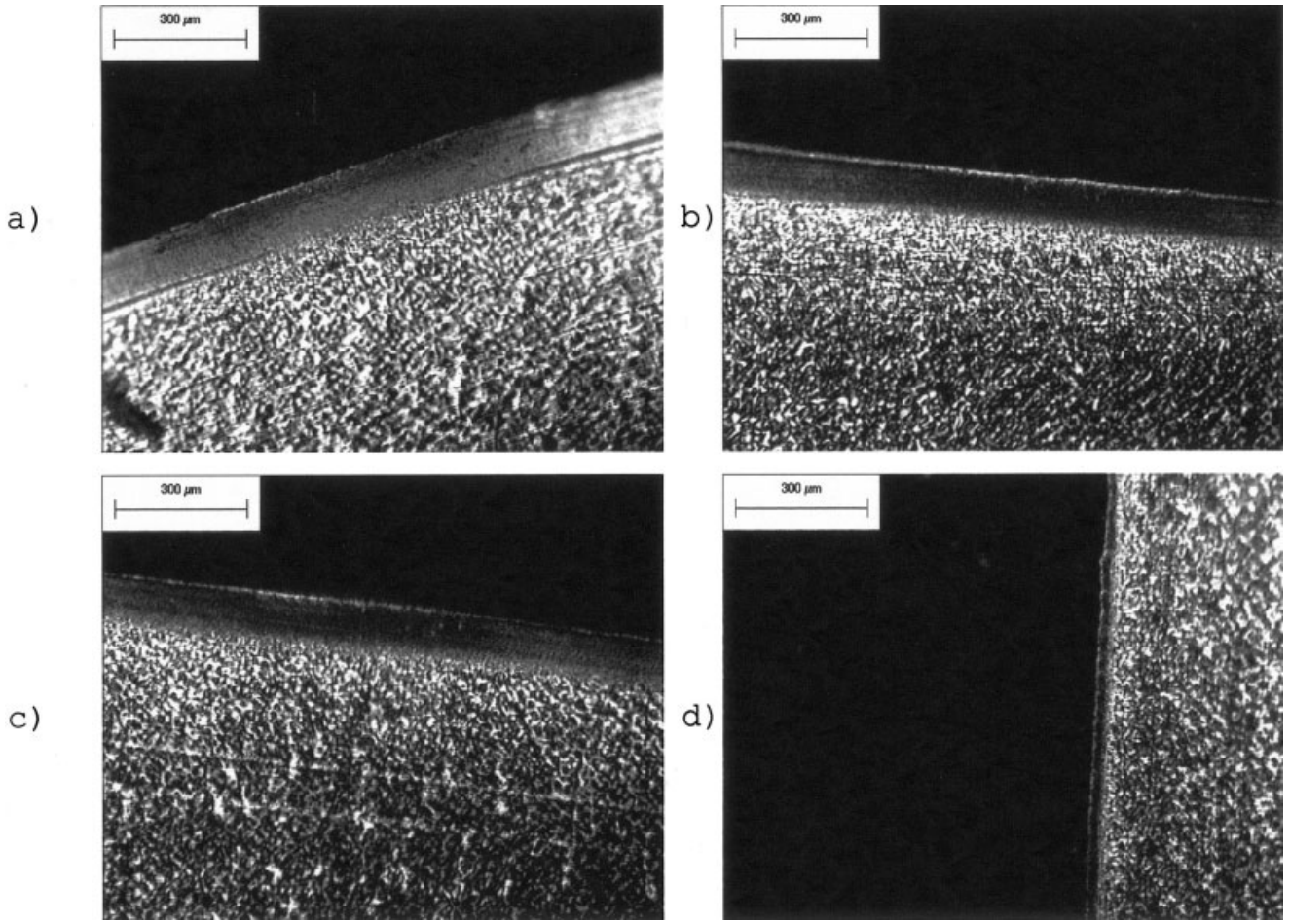


**Figure 11** Samples extruded at $T_d$ = 200°C and $Q$ = 8.9 kg/h. Area numbers: (a) 2, (b) 4, (c) 6, (d) 8.

Figure 8 shows plots of the thickness of the shear-induced crystallized layer as a function of the position along the die at different $T_d$'s. This layer was assumed to end at the point where the spherulitic morphology begun (layer 1 in Fig. 9). Area number 1 was disregarded because, being near the die entrance, it would probably have shear and elongational flows components.

As said before, two situations are going to be analyzed: (1) constant $Q$ with increasing $T_d$ and (2) constant $T_d$ with increasing $Q$. The first situation was analyzed by using area number 6 as a reference. The results are shown in Table II, where the values of the thickness as a function of $T_d$ at a given $Q$ are also shown.

It can be observed that at $Q$ = 4.3, 7.75, and 10.05 kg/h, the thickness of the shear-induced crystalline layer decreased with the increase of $T_d$, as predicted.

To analyze the second situation, that is, constant $T_d$ with increasing $Q$, the same area number was chosen. The results are shown in Table III.

It can be observed that at a given $T_d$, as $Q$ increased, the thickness of the shear-induced layer increased, as also predicted.

Regarding the die length, it was also observed that, at 169°C, the thickness of the flow-induced crystalline layer increased with the length as also predicted by the Janeschitz-Kriegl theory.[4] At the other temperatures, a critical flow rate, 6.6 kg/h, was found, below which the thickness of the shear-induced layer increased with the die length at all temperatures. Above this critical flow rate, the thickness of the flow-induced layer decreased with the die length, probably due to rapid relaxation of the molecules.

### Polarized light optical microscopy

Figure 9 shows a PLOM of a whole sample with thickness of approximately 1.5 mm; five different layers, from the wall to the center, can be visualized: a highly oriented layer (without apparent crystallinity, layer 1); a highly crystalline and dense region (layer 2); a crystalline but less dense layer (layer 3); a crystalline and still less dense layer (layer 4); and a crystalline and more dense region (layer 5). Table IV shows the approximated thickness of each layer for this sample.

Figure 10 shows PLOM micrographs of layers 1 and 2 as a function of the die length; as already mentioned,

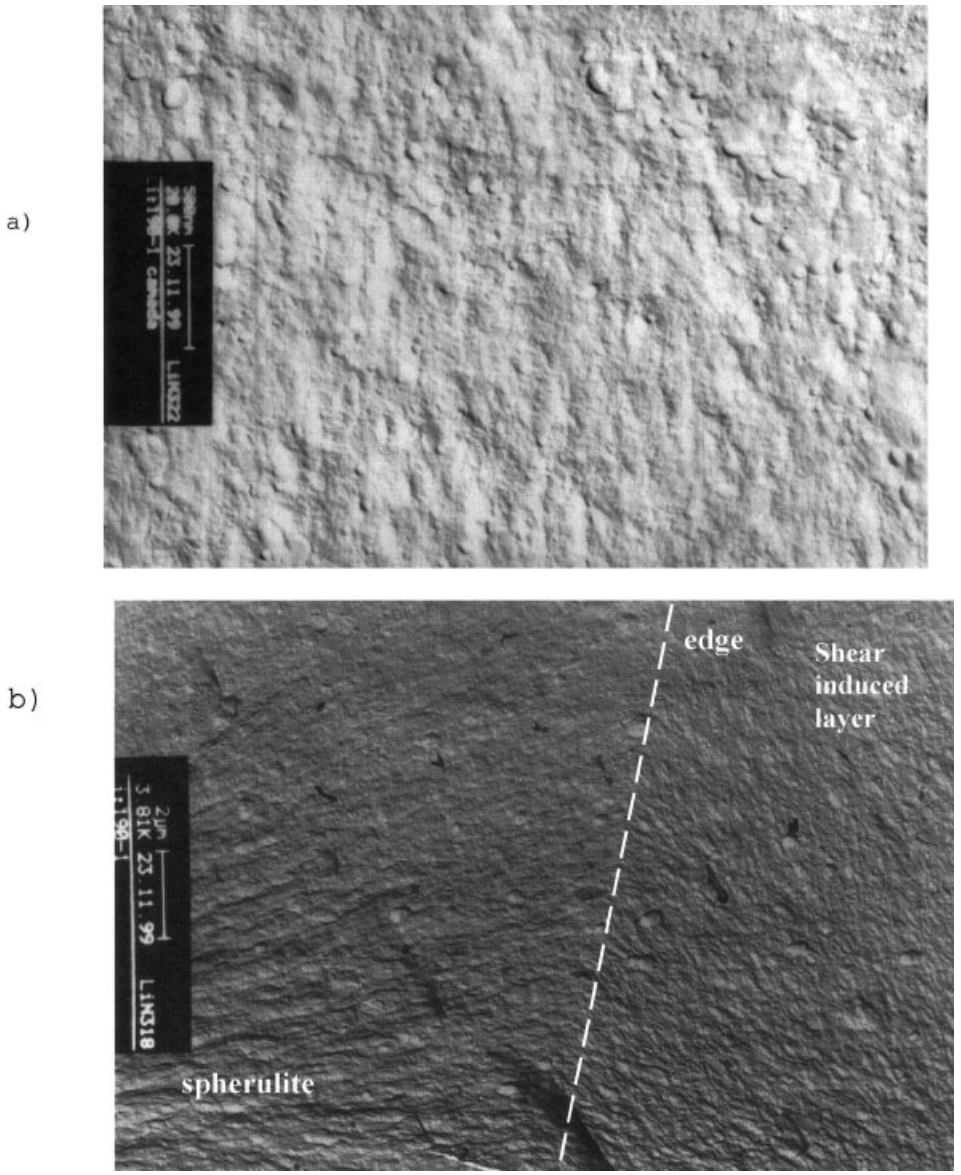


**Figure 12** TEM micrographs of the interface between layers 1 and 2: (a) sample extruded at 200°C, area number 7, $Q = 7.5$ kg/h; (b) sample extruded at 190°C, area number 7, $Q = 8.0$ kg/h.

layer 1 increased with the die length at $T_d = 169$°C at all the flow rates.

Figure 11 also shows PLOM micrographs of layers 1 and 2, at $T = 200$°C and at $Q = 8.9$ kg/h; in this case, it is observed that the thickness of layer 1 decreased with the die length, when $Q > 6.6$ kg/h.

### Scanning and transmission electron microscopy

Figure 12 shows TEM micrographs of the interface between layers 1 and 2; Figure 12(a) is the interface of a sample extruded at 200°C, area number 7, $Q = 7.5$ kg/h, and Figure 12(b) is the interface of a sample extruded at 190°C, area number 7, $Q = 8.9$ kg/h.

In the sample shown in Figure 12(b), a well-defined interface can be observed; the orientation of both layers forms a 90° angle between themselves. Figure 13 shows SEM micrographs of this sample.

It can be observed that layer 2 is formed mainly by spherulites; on the other hand, layer 1 is formed by highly oriented lamellae. To study the crystalline phases that form these morphologies, studies of WAXS were also made.

### Wide-angle x-rays

Figure 14 shows X-ray diffraction of the surfaces of some of the extruded samples at different $T_d$'s. It can be observed that the diffraction of all the samples is similar, having peaks and corresponding crystalline planes[10] as shown in Table V.

It can also be observed that the peak corresponding to the $\beta$-phase is more intense in the surface of the

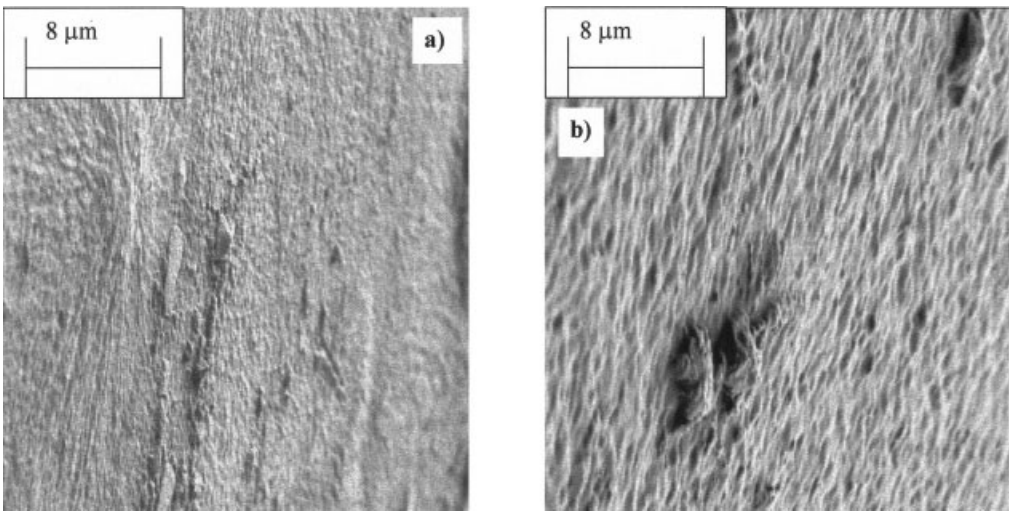


**Figure 13** SEM micrographs of samples extruded at $T_d$ = 190°C, $Q$ = 7.75 kg/h, area number 7, magnification ×5000: (a)Region 2 and (b) Region 1.

sample extruded at $T_d$ = 200°C, probably because the cooling rate was higher at this temperature, as said before, and $T_{\beta\alpha}$ was reached quicker than at the other $T_d$'s.

To study layers 1 and 2, layers of different thicknesses were removed from the original surface, and the resulting surfaces were X-ray diffracted; the results are shown in Figure 15.

It can be observed from this figure, that, as the layers are removed, the intensity of the $\alpha$-phase decreased, because of the decrease in orientation. Regarding the $\beta$-peak, it can also be observed that this phase disappeared when a layer of 181 $\mu$m was removed from the surface.

The X-ray penetration in a polymer can be calculated from the equation[21]

$$\frac{I}{I_0} = e^{-\mu t} = e^{-\mathrm{MAC}\rho t} \tag{4}$$

where $I$ is the transmitted intensity, $I_0$ is the incident intensity, $\mu$ is the linear absorption coefficient of the polymer, $t$ is the thickness of the sample (or penetration thickness), MAC is the mass absorption coefficient, and $\rho$ is the density of the polymer.

The MAC can be calculated from ref. 22, being equal to 4.001; if we assume that $\rho$ = 0.9, then at $2\theta$ = 16° ($\beta$-phase), $t$ = 891 $\mu$m.

Therefore, by using eq. (4), the X-ray penetration after the removal of the layers can be calculated. These values are shown in Table VI.

It can be observed that even after the removal of the larger layer (255 $\mu$m), the X-rays did not penetrate into

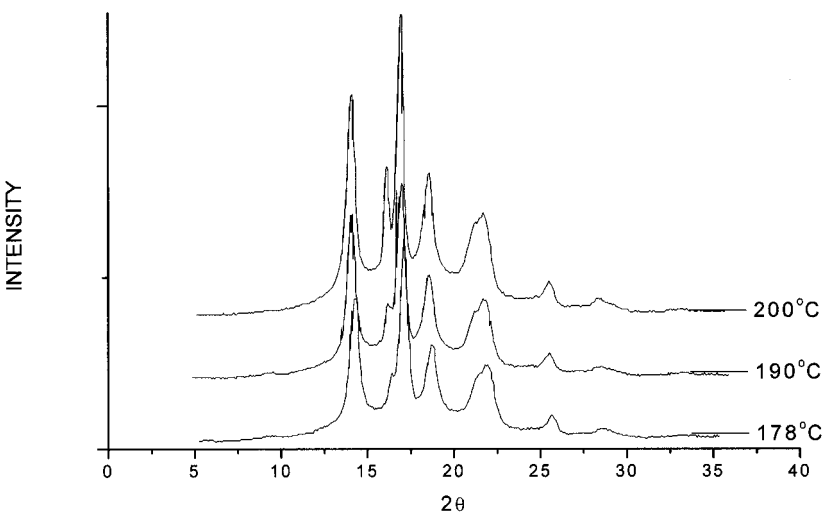


**Figure 14** X-ray diffraction of the surfaces of the extruded samples at different die temperatures.

**TABLE V**
**X-ray Diffraction of the Surfaces**

| Main peak (2θ), ° | Crystalline plane | i-PP phase |
|---|---|---|
| 14 | 110 | α |
| 16 | 300 | β |
| 17 | 040 | α |
| 18.5 | 130 | α |
| 21 | 111 | α |
| 21 | 301 | β |
| 22 | 131, 041 | α |

**TABLE VI**
**X-ray Penetration as a Function of the Thickness of the Removed Layers**

| Thickness of the removed layer (μm) | X-ray penetration (μm) | Height of the β-peak (mm) |
|---|---|---|
| 0 | 891 | 1.9 |
| 58 | 949 | 1.5 |
| 118 | 1009 | 0.8 |
| 181 | 1072 | 0.1 |
| 255 | 1146 | 0 |

layers 1′, 2′, and 3′. Therefore, the X-ray diffraction shown in Table VI corresponds approximately to the diffraction of layers 1 to 4′. It is also observed that the height of the β-peak decreased as from the surface toward the center of the sample, being more intense at the original surface and disappearing after a layer of 181 μm was removed, which corresponds approximately to the removal of layers 1 and 2. Thus, within experimental error, we can conclude that the majority of the β-phase was located in these two regions. However, if we observe also the PLOM micrographs, we will see that the more highly birefringent spherulites were located in region 2. If there were β-crystallites in layer 1, probably they were very small and could not be seen by PLOM. Therefore, we can conclude that layer 2 was mainly composed of the β-phase, while layer 1 was mainly composed of very small and highly oriented α-cylindrites (which could not be seen by PLOM, but could be seen by SEM and TEM), as the Varga and Karger-Kocsis model[12] suggests. We can also observe that the intensity of the β-peak decreased from the top surface to the center, following the same trend that the shear rate profile. In other words, the amount of β-phase decreased as the shear rate decreased. This same behavior was found in recent works.[13,17]

## CONCLUSION

The characterization of i-PP shear-induced crystalline layers developed in a slit die was done by different techniques, drawing the following conclusions.

1. From the rheological studies, a four-regions curve of shear stress versus shear time was obtained, as predicted by the McHugh et al. model, when a coupling parameter $\xi = 2$ is used. Also, it was observed that at a given $T_c$, the induction time decreased as the shear rate increased, and at a given shear rate, the higher the $T_c$, the higher the induction time.

2. After extrusion through the slit die, it was observed that, at a given $Q$, the thickness of the shear-induced crystalline layer decreased with the increase of $T_d$, as predicted; on the other hand, at a given $T_d$, the

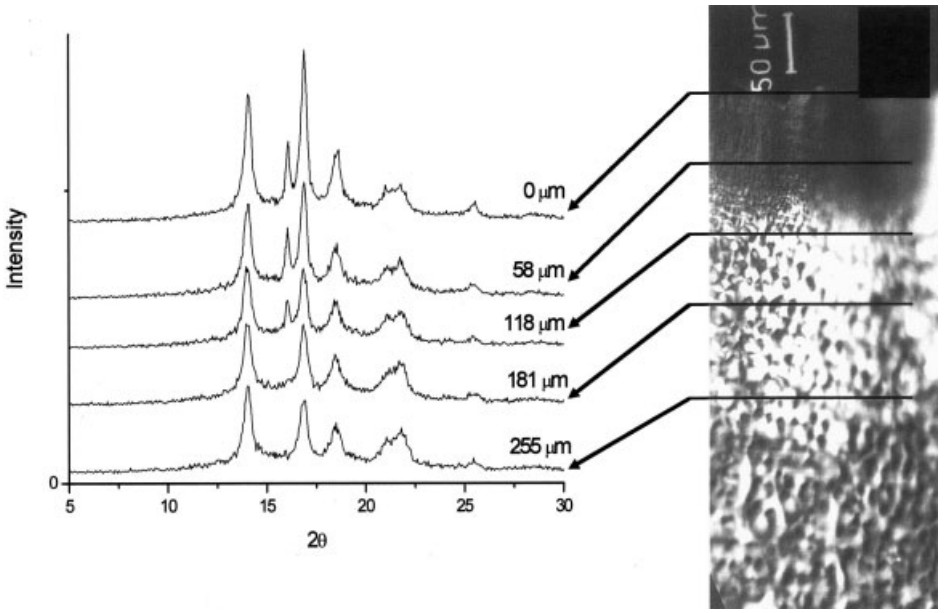


**Figure 15** X-ray diffraction of the surfaces as a function of the thickness of the removed layers.

thickness of this layer increased as $Q$ increased, as also predicted. Only at $T_d = 169°C$, it was observed that the thickness of this layer increased with the die length, as predicted by the Janeschitz-Kriegl et al. theory.

3. From PLOM, five different layers along the thickness of the sample were observed. From SEM and TEM, it was found that layer 2 was spherulitic, while layer 1 was formed by highly oriented lamellae.

4. From the X-ray studies, it was found that the highest amount of $\beta$-phase was located in layers 1 and 2 and that the amount of this phase decreased as the shear rate decreased. Coupled with the PLOM, SEM, and TEM results, we concluded that layer 2 was mainly composed of $\beta$-spherulites, while layer 1 was mainly formed by very small and highly oriented $\alpha$-crystallites, as the Varga and Karger-Kocsis model suggested.

This article is dedicated to the late Prof. J. Petermann, from University of Dortmund, for his kindness and encouragement. The authors also thank FAPESP and PRONEX for financial aid and to Prof. P. I. Paulin F for helpful discussions on X-rays diffraction.

## References

1. da Silva, L. B.; Bretas, R. E. S. Polym Eng Sci 2000, 40, 1414.
2. Lagasse, R. R.; Maxwell, B. Polym Eng Sci 1976, 16 (3), 189.
3. Lamberti, G.; Titomanlio, G. Flow-Induced Crystallization in Film Casting Experiments; May 21–24, 17th Annual Meeting; Polym Proc Soc; 2001.
4. Eder, G.; Janeschitz-Kriegl, H.; Liedauer, S. Prog Polym Sci 1990, 15, 629.
5. Doufas; A. K.; Dairanieh, I. S.; McHugh, A. J. J Rheol 1999, 43, 85.
6. Varga, J. J Mater Sci 1992, 27, 2557.
7. Carvalho, B.; Bretas, R. E. S. J Appl Polym Sci 1998, 68, 1159.
8. Carvalho, B.; Bretas, R. E. S. J Appl Polym Sci 1999, 72, 1733.
9. Meille, S. V.; Ferro, D. R.; Bruckner, S.; Lovinger, A. J.; Padden, F. J. Macromolecules 1994, 27, 2615.
10. Vleeshouwers, S. Polymer 1997, 38 (13), 3213.
11. Padden, F. J.; Keith, H. D. J Appl Phys 1979, 30, 1479.
12. Varga J, J.; Karger-Kocsis, J. J Polym Sci, Part B: Polym Phys 1996, 34, 657.
13. Nogales, A.; Hsiao, B. S.; Somani, R. H.; Srinivas, S.; Tsou, A. H.; Balta Calleja, F. J.; Exquerra, T. A. Polymer 2001, 42, 5247.
14. Riekel, C.; Karger-Kocsis, J. Polymer 1999, 40, 541.
15. Vleehouwers, S.; Meijer, H. E. H. Rheol Acta 1996, 35, 391.
16. Nagatake, W.; Takahashi, T.; Masuuchi, Y.; Takimoto, J. I.; Koyama, K. Polymer 2000, 41, 523.
17. Chaudhry, B. I. Ph.D. Thesis, PPG-CEM, DEMa-UFSCar, 2002; p. 65.
18. Isayev, A. I.; Chan, T. W.; Shimojo, K.; Gmerek, M. J. J Appl Polym Sci 1995, 55, 807.
19. White, J. L. Principles of Polymer Engineering Rheology; Wiley: New York, 1990.
20. Bretas, R. E. S.; Davila, M. A. Reologia de Polímeros Fundidos; EDUFSCar, São Carlos, 2000.
21. Alexander, L. E. X-rays Diffraction Methods in Polymer Science; Wiley Interscience: New York, 1969.
22. http://www.ccp14.ac.uk/ccp/web-mirrors/bca-spreadsheets" _www.ccp14.ac.uk/ccp/web-mirrors/bca-spreadsheets_.